Proceedings of the 2013 Industrial and Systems Engineering Research Conference
A. Krishnamurthy and W.K.V. Chan, eds.

Functionally Gradient Tissue Scaffold Design and Deposition Path Planning for Bio-additive Processes

AKM Khoda[1], Ibrahim T. Ozbolat[2] and Bahattin Koc [1,3]

[1]Department of Industrial Engineering, University at Buffalo, Buffalo, NY 14260, USA
[2]Department of Mechanical and Industrial Engineering, Center for Computer Aided Design, The University of Iowa, Iowa City, IA 52242-1527, USA
[3]Faculty of Engineering and Natural Sciences, Sabanci University, Istanbul 34956, Turkey

Abstract

A layer-based tissue scaffold is designed with heterogeneous internal architecture. The proposed layer-based design uses a bi-layer pattern of radial and spiral layer consecutively to generate functionally gradient porosity following the geometry of the scaffold. Medial region is constructed from medial axis and used as an internal geometric feature for each layer. The radial layers are generated with sub-region channels by connecting the boundaries of the medial region and the layer's outer contour. Proper connections with allowable geometric properties are ensured by applying optimization algorithms. Iso-porosity regions are determined by dividing the sub-regions into pore cells. The combination of consecutive layers generates the pore cells with desired pore sizes. To ensure the fabrication of the designed scaffolds, both contours have been optimized for a continuous, interconnected, and smooth deposition path-planning. The proposed methodologies can generate the structure with gradient (linear or non-linear), variational or constant porosity that can provide localized control of variational porosity along the scaffold architecture. The designed porous structures can be fabricated using bio-additive fabrication processes.

Keywords

Scaffold architecture, gradient porosity, biarc fitting, continuous path planning, bio-additive manufacturing

1. Introduction

The porous internal architecture of the scaffold may have significant influence on the cellular microenvironment and tissue re-generation process in tissue engineering applications [1]. However, limited nutrient and oxygen supply from and to the scaffold architecture has been reported in both static [2] and dynamic [3] environments. As a result, the seeded cells away from the peripheral boundary of the scaffold have lower survival rates and tissue formation. Controlling the size, geometry, orientation, interconnectivity, and surface chemistry of pores and channels could determine the nature of nutrient flow [4]. Therefore, it is important to change and control the porosity along the architecture of the scaffold, and at the same time, it should have the channels feeding deepest regions of the scaffold for proper nutrition flow and waste removal. Thus, the need for a reproducible and fabricatable structure design with controllable gradient porosity is obvious but possibly limited by design and fabrication methods [5-7].

Variational porosity design has been used by Lal *et al*. [8] in their proposed microsphere-packed porous scaffold modeling technique. The resultant porosity is stochastically distributed throughout the structure. A heuristic-based porous structure modeling has been developed in the literature [9] using an approach based on constructive solid geometry (CSG) with stochastic Boolean functions. Porous objects designed with a nested cellular structure have been proposed in the literature [10], which may introduce the gradient porosity. In [11], geometric modeling of functionally graded material (FGM) has been developed with graded microstructures. The gradient porosity in the FGM has been achieved with stochastically distributed Voronoi cells. Porous scaffolds with 3D internal channel networks are designed with axisymmetric cylindrical geometry based on energy conservation and flow analysis [12, 13]. After the scaffolds are designed, they need to be fabricated mainly by using bio-additive processes layer by

layer. The filament deposition direction or the layout pattern in scaffold plays an important role towards its mechanical and biological properties as well as cell in-growth [14]. In the literature, because most of the design and fabrication processes are not developed simultaneously, and their fabrications are after-thought, the designed scaffolds might generate discontinuous deposition path which may not be feasible for bio-additive processes.

In this paper, we propose a novel method to addresses the scaffold design limitations by designing a functionally gradient variational porosity architecture that conforms to the anatomical shape of the damaged tissue. The proposed layer-based design uses a bi-layer pattern of radial and spiral layers consecutively in 3D to achieve the desired functional porosity. The material deposition is controlled by the scaffold's contour geometry, and this would allow us to control the internal architecture of the designed scaffold. The designed layers have been optimized for a continuous, interconnected, and smooth material deposition path-planning for bio-additive fabrication processes.

2. Porosity modeling

For implementing the methodology, the anatomical 3D shape of the targeted damaged area need to be extracted via non-invasive technique. Firstly, medical image obtained from Computed Tomography (CT), Magnetic Resonance Imaging (MRI) is used to get the geometric and topology information of the replaced tissue. The three dimensional geometric model is then sliced by a set of intersecting planes parallel to each other to find the layer contours which are suitable for additive manufacturing processes. All contour curves are simple planner closed curve and the general equation for these contour can be parametrically represent as-

$$\begin{aligned} C_i(t_i) &= (x(t_i), y(t_i)) \qquad \forall i = 0,...m \\ t_i &\in [a_i, b_i] \\ C_i(a_i) &= C_i(b_i) \end{aligned} \tag{1}$$

Here, $C_i(t_i)$ represent the parametric equation for i^{th} contour with respect to parameter t_i at a range between $[a_i, b_i]$.

2.1 Medial region generation

As mentioned above, the seeded cells away from the peripheral boundary of the scaffold have lower survival rates and tissue formation. In our proposed design processes, the spinal (deepest) region of the scaffold architecture needs to be determined so that the gradient of functional porous structure can change between the outer contour and the spinal region. The medial axis of each layer contour C_i is used as its spine or internal feature. A medial axis M_i for every planar closed contour or slice C_i has been generated using the inward offsetting method [15] as shown in Figure 1(a). The approximated offset curve $C_i^d(t)$ of the contour curve $C_i(t)$ at a distance d from the boundary is defined by:

$$C_i^d(t) = C_i(t) + d\vec{N}(t) \tag{2}$$

where $\vec{N}(t)$ is the unit normal vector on curve $C_i(t)$ at a parametric location t . To ensure the proper physical significance of this one-dimensional geometric feature, a medial region has been constructed from the medial axis for each corresponding layer as shown in Figure 1(b). The medial region has been defined as the sweeping area covered by a circle whose loci of centers are the constructed medial axis. The width of this medial region is determined by the radius of the imaginary circle. Higher width can be used if the scaffold is designed with perfusion bioreactor cell culture consideration to reduce the cell morbidity with proper nutrient and oxygen circulation. The boundary curve of the medial region is defined as the medial boundary in this paper; it is also the deepest region from the boundary, as shown in Figure 1(b).

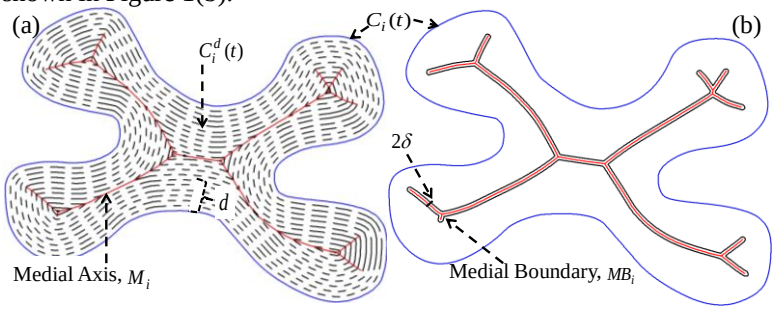

Figure 1 (a) The medial axis, and (b) medial boundary generation.

2.2 Radial sub-region construction

In traditional bio-additive processes, materials are deposited as filaments following a Cartesian layout pattern (0^0-90^0) in each layer crisscrossing the scaffold area arbitrarily. After cells are seeded in those filaments, their accessibility to the outer region for nutrient or mass transport becomes limited to the alignment of the filament in lieu of their own locations. Besides, the seeded cells in-growth direction does not match the filament layout pattern. This could affect the cell survival rate significantly as discussed earlier. However, a carefully crafted filament deposition between the outer contour and the medial region can match the cell in-growth direction and increase the mass transportation at any location as shown in Figure 2(b).

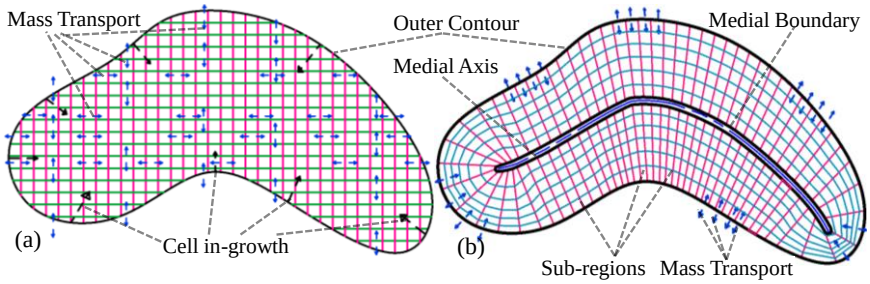

Figure 2 Mass transport and cell in-growth direction in (a) traditional layout pattern, and (b) proposed radial pattern.

To improve the mass transportation for the seeded cells inside the scaffold, such an internal feature can be used as a base to build radial channels that can be used as a guiding path for nutrient flow. These radial channels are defined as sub-regions in this paper as shown in Figure 2(b). A two-step sub-region modeling technique is developed to increase the accessibility and mass transportation for the designed sub-region in this section. During modeling, the scaffold area is decomposed into smaller radial segments by ensuring global optimum accessibility between the external contour $C_i(t)$ and the medial region $MB_i(t)$. Then, a heuristic method is developed to construct the radial sub-regions by accumulating those segments.

2.2.1 Decomposing the scaffold architecture into segments with ruling line generation

To construct the radial channels or sub-regions, the scaffold area is decomposed into a finite number of segments connected between the external contour $C_i(t)$ and the internal feature $MB_i(t)$. The space between the two lines is defined as a segment. To increase accessibility, and to ensure the smooth property transition between the outer and inner contours, an adaptive ruled layer algorithm [15] is developed to discretize the scaffold area as shown in Figure 3. In order to connect both the external contour curve $C_i(t)$ and the internal medial boundary contour $MB_i(t)$, they are parametrically divided into independent number of equal cord length sections. To ensures a better resolution and distribution of inserted ruling lines and avoids overlapping one-to-one point insertion technique [15] is implemented as shown in Figure 3. As a result on the external contour curve $C_i(t)$, a total N_1 number of points are generated as $P_C = \{p_{cj}\}_{j=0,1..N_1}$, where $p_{cj} = C_i(t_j)$ and $t_j \in [a_i, b_i]$. Similarly, the same number of points are generated on the internal medial boundary $MB_i(t)$ and represented as $P_m = \{p_{mk}\}_{k=0,1..N_1}$, where $p_{mk} = MB_i(t_k)$ and $t_k \in [A_i, B_i]$.

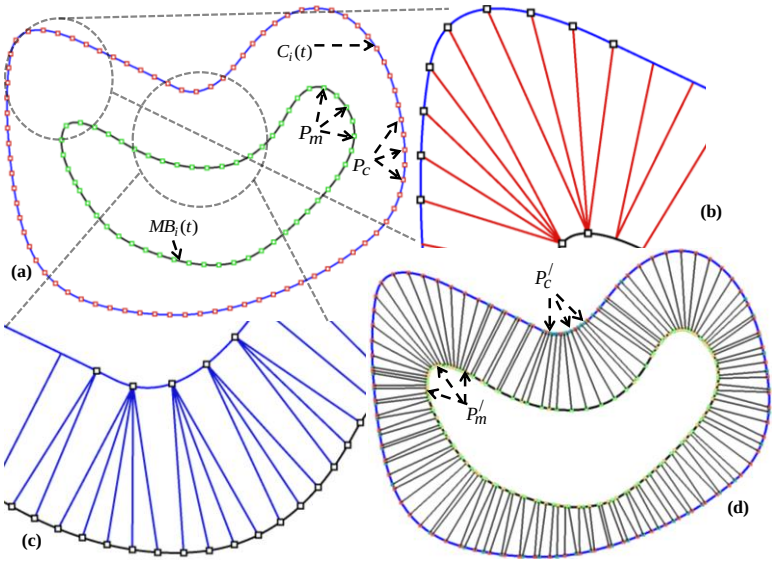

Figure 3 (a) Point insertion with equal cord length; multiple-to-one counterpoint from (b) $C_i(t)$ to $MB_i(t)$ (c) $MB_i(t)$ to $C_i(t)$ and (d) one-to-one point generation.

A global optimization model is formulated for point matching between two directrices to connect the ruling lines where the objective is to maximize the sum for all N_1 number of points.

$$Maximize \sum_{j=0}^{N_1}\sum_{k=0}^{N_1} \frac{\overrightarrow{N(p_{cj})}.\overrightarrow{N(p_{mk})}}{\left|p_{cj}\ p_{mk}\right|^2} \tag{3}$$

Subject to:

$$LR_s : \{\overline{p_{cj}\,p_{mk}} \cap C_i(t)\} = \{p_{cj}\} \qquad \forall j,k \tag{4}$$

$$LR_s : \{\overline{p_{cj}\,p_{mk}} \cap MB_i(t)\} = \{p_{mk}\} \qquad \forall j,k \tag{5}$$

$$LR_s : \{\overline{p_{cj}\,p_{mk}} \cap LR_{s-1}\} = \varnothing \qquad \forall j,k,s \tag{6}$$

During ruling line insertion, they should intersect with the base curve only at one single point $C_i(t)$ and $MB_i(t)$ as shown Equation (4) and (5) to avoid twisting and intersecting ruling lines. Moreover, they should not intersect with each other because intersection generates invalid discretization as the same area given in Equation (6).

2.2.2 Accumulating segments into sub-region

An orderly and incremental sub-region accumulation has been performed, and the goal is to accumulate the segment sets LS into as few sub-regions SR_d as possible. For uniform geometry, every segment that arrives in the queue may have identical segment i.e. the similar variable values. In such a case, there is no uncertainty and the equal number of segments can be bundled to construct the sub-region. However, for free form geometry, the generated segments constructed by the ruling lines are anisotropic in nature and sub-region constructed must meet the corresponding geometric dimension RA^*, RL^* and RU^* during their accumulation as presented in Equation (7).

$$\text{Min} \quad \sum_d \omega_a\left(\left|RA_d - RA^*\right|\right) + \omega_l\left(\left|RL_d - RL^*\right|\right) + \omega_u\left(\left|RU_d - RU^*\right|\right) \quad \forall \quad d \tag{7}$$

Here, RA_d represent the area, RS_d is the lower width and RU_d is the upper width as shown in Figure 4(a). The accumulation of the sub-region is geometrically determined with the following algorithm:

(a) The segments are obtained from an initial set $LS = \{ls_n\}_{n=0,1..N}$.

(b) Start with any segment as initial segment ls_i and add the consecutive segment $ls_{(i+1)}$ into the end of the queue.

(c) Determine their accumulation following their properties $SR_d = \{RA_d, RL_d, RU_d\}$.

If ($RA_d \approx RA^*; RL_d \approx RL^*; RU_d \approx RU^*$) /*** The variables satisfy the acceptable property range***/
Then
{ Cut the queue;
Add penalty cost to the objective value in the Equation (7);
Accumulate the sub-region, and Start a new queue; }

If ($RA_d < RA^*; RL_d < RL^*; RU_d < RU^*$) /*** The variables properties are short of the acceptable property range***/
Then
{ Add a consecutive segment to the queue; }

If ($RA_d > RA^*; RL_d > RL^*; RU_d > RU^*$) /*** The variables properties are above the acceptable property range***/
Then
{ Cut the queue to the previous segment;
Add penalty cost to the objective value in the Equation (7);
Start the new queue with the current segment as the initial segment }

(d) Continue step (c) until all N segments are accumulated.

(e) Change the initial segment $i \leftarrow (i+1)$: $(i+1) < N$ and continue the processes (step (a) to (d)) to find the minimum objective function value.

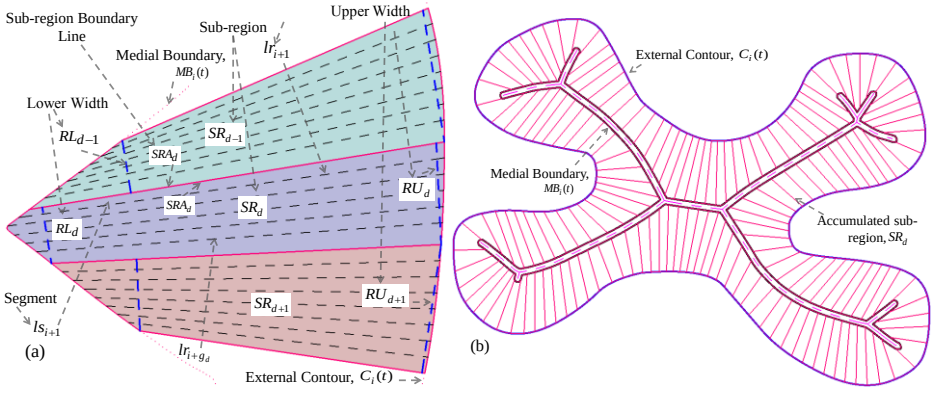

Figure 4 (a) Sub-region's geometry and construction from segments, and (b) discretizing the scaffold area with sub-regions.

After implementing the proposed heuristic algorithm, a set of sub-regions $SR = \{SR_d\}_{d=0,1..D}$, where D is the number of sub-regions, has been constructed with a compatible lower and upper width geometry. Each sub-region preserves a section for both the external contour curve $C_i(t)$ and the internal medial boundary feature $MB_i(t)$ along its lower and upper boundaries as shown in Figure 4(a). The generated sub-regions discretizing the scaffold area are shown in Figure 4(b).

2.3 Iso-porosity region generation

Since the properties or the functionality of scaffolds are changing towards the inner region, the designed porosity has to follow the shape of the scaffold. Thus iso-porosity regions are introduced which will follow the shape of the scaffold as shown in Figure 5(a). To build the iso-porosity region each sub-region is partitioned according to the porosity with iso-porosity line segments as shown in Figure 5(b). The porosity has been interpreted into area by modeling the pore cell $PC_{d,p}$ methodology discussed in our previous work [16], where, $PC_{d,p}$ is the p^{th} pore cell in the d^{th} sub-region SR_d .

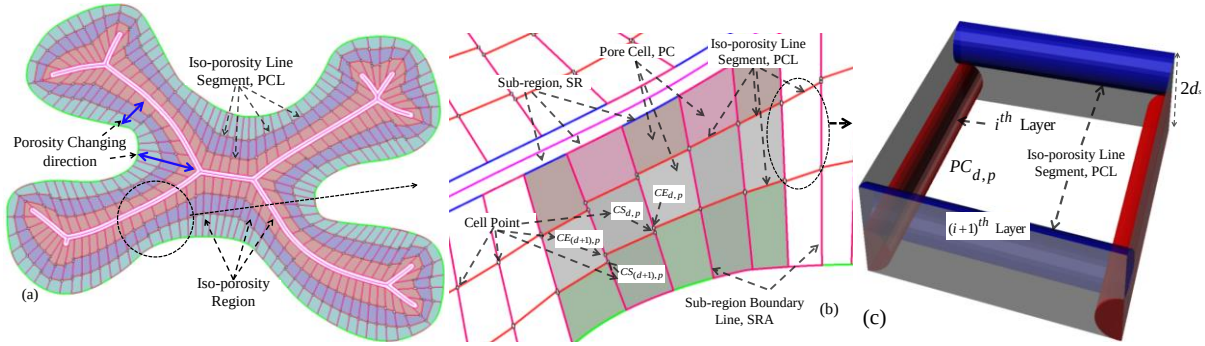

Figure 5 (a) Partitioning the sub-regions by iso-porosity line segments (PCL) (b) zoomed view, and (c) a single pore cell.

The desired porosity has been interpreted into area and the sub-regions are divided accordingly. The acceptable pore size reported in the literature [17] consider isotropic geometry, i.e., sphere, cube or cylinder. Because of the free-form shape of the outer contour and the accumulation pattern, the generated sub-regions will have anisotropic shapes as shown in Figure 4(b). Thus, the acceptable pore size needs to be calculated from the approximating sphere diameter [16]. An optimization method [16] is used to divide the sub-regions into pore cell considering the area conservation rule. Moreover, the porosity in each pore cell with the same numerical location at any sub-region is the same. Thus the desired controllable porosity gradient can be achieved with iso-porosity region constructed by the pore cells. The height $2d_s$ of the pore cell is the same as the height of the two layers i.e. two times the diameter of the filament as shown in Figure 5(c). By stacking successive i^{th} and $(i+1)^{th}$ layers, a 3D fully interconnected and continuous porous architecture is achieved. Moreover, the iso-porosity line segments cross at the support points for sub-regions above, which has been widely used in layer-by-layer manufacturing, as each layer supports the consecutive layer. Connecting the cell point, $CS_{d,p}$ and $CE_{(d+1),p}$ of all iso-porosity line segments (PCL) gradually will generate a piecewise linear iso-porosity curve shown in Figure 5.

3. Optimum deposition path planning

The proposed bi-layer pore design represents the controllable and desired gradient porosity along the scaffold architecture. To ensure the proper bio-additive fabrication, a feasible tool-path plan needs to be developed that would minimize the deviation between the design and the actual fabricated structure.

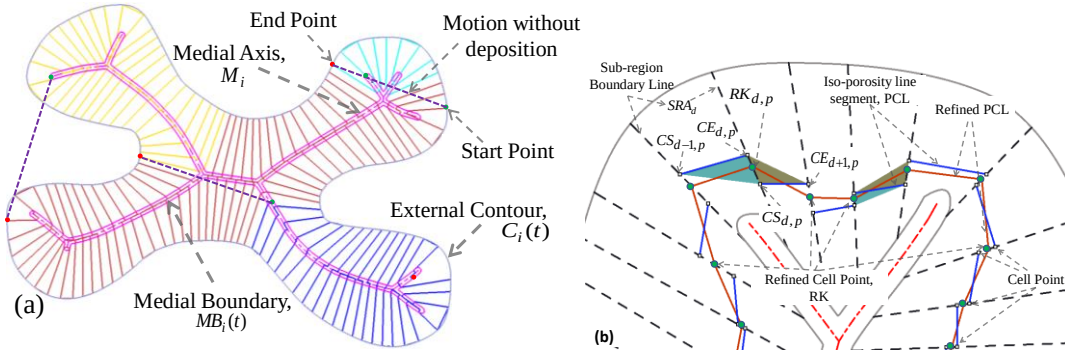

Figure 6 (a) Simulation of tool-path for fabrication along with start and stop points and motion without deposition (b) Cell point refinement.

3.1 Deposition-path plan for sub-regions

To generate the designed sub-regions in the i^{th} layer, the tool-path has been planned through the sub-region's boundary lines, SRA, and bridging the medial region to generate a continuous material deposition path-plan. Crossing the medial region along the path-plan will provide the structural integrity for the overall scaffold architecture and divide the long medial region channel into smaller pore size. Thus, at first we extended the sub-region's boundary lines, SRA towards the medial axis crossing the medial region and then a path-planning

algorithm has been developed to generate the continuous path for the sub-region layer fabrication. An algorithm has been developed to generate a continuous tool-path through the the sub-region's boundary lines, SRA, considering the minimum amount of over-deposition as well as starts and stops, as shown in Figure 6(a) [15].

3.2 Deposition path for iso-porosity layer

As shown in Figure 5(a), the iso-porosity curve is closed but not smooth and for a better fabrication results iso-porosity curve needs to be smoothed. The iso-porosity curve in the $(i+1)^{th}$ layer can be constructed as a set of piecewise line segments through the inserted cell points $CS_{d,p}$ and $CE_{(d+1),p}$ as shown in Figure 5(b); however, this can cause discrete deposited filaments because of the stepping and needs to be smoothed for a uniform deposition. Besides, the number of points on the iso-porosity curve requires a large number of tool-path points during fabrication. Linear and circular motion provides better control of the deposition speed along its path precisely for bio-additive manufacturing processes. Thus, a curve-fitting methodology is used to ensure a smooth and continuous path. However, the distribution of cell points may not be suitable for curve fitting techniques, i.e., each sub-region's boundary line contains two adjacent cell points and this can skew curve fitting unexpectedly. Instead, a two-step smoothing for iso-porosity path is proposed to achieve a continuous tool-path suitable for fabrication. The first step refines the cell point distribution and a biarc fitting technique has been developed then to generate C^1 continuity in iso-porosity region path planning.

3.2.1 Cell point refinement

The iso-porosity curve generated from connecting the gradual cell points could have a stepping due to two cell points $CS_{d,p}$ and $CE_{d,p}$ $\forall\, d\,;\, p$ on the same sub-region boundary lines SRA_d $\forall$ d . An area weight-based point insertion algorithm has been developed to generate the refined cell points, $RK_{d,p}$. Mathematically, the location of this weighted point $RK_{d,p}$ can be expressed as:

$$RK_{d,p} = CE_{d,p} + w\left|CS_{d,p}CE_{d,p}\right|\frac{\overrightarrow{CS_{d,p}CE_{d,p}}}{\left\|\overrightarrow{CS_{d,p}CE_{d,p}}\right\|} \tag{8}$$

Here, the weight, *w* represents the ration $\dfrac{\text{Area\_}(CS_{d-1,p}CS_{d,p}CE_{d,p})}{\text{Area\_}(CS_{d-1,p}CS_{d,p}CE_{d,p}) + \text{Area\_}(CE_{d+1,p}CS_{d,p}CE_{d,p})}$ shown in Figure 6(b). Connecting these weighted point $RK_{d,p}$ consecutively would form a piecewise closed linear curve as shown in Figure 6(b). This will eliminate the stepping issue but could result in over-deposition at the refined cell points because of possible directional changes.

3.2.2 Smoothing iso-porosity curves with biarcs

A planar iso-porosity curve with C^1 continuity could provide the required smoothness while maintaining the iso-porosity regions. Thus a bi-arc fitting through those refined cell points would be more appropriate for a smooth deposition path. The following information is required to construct biarc [15]:

(a) The number of points (D) through which it must pass.

(b) The coordinate (x_i, y_i) of the point $RK = \{RK_{d,p}\}_{d=0,1..D;\ p=0,1..(P-1)}$.

(c) The tangent at the first and last points.

The iso-porosity curve is generated by initializing the tool-path at the first refined cell point $RK_{d=1} \rightarrow RK_s$. Then a biarc is fitted for the point set $PS = \{RK_d, RK_{d+1}, RK_{d+2}\}$, and the fitting accuracy of a biarc has been determined based on the one–sided Hausdorff distance [18]. Even though, the biarc has been constructed from the point set RK, the fitting accuracy must be measured from the actual cell point set $CS = \{CS_{d,p}\}_{d=0,1..D;\ p=0,1..(P-1)}$ and $CE = \{CE_{d,p}\}_{d=0,1..D;\ p=0,1..(P-1)}$ to maintain minimum deviation from the actually computed pore size as shown in Figure 10. The Hausdorff distance provides a robust, simple and computationally acceptable curve-fitting quality measure methodology and can produce a smaller number of biarcs from the cell points. The continuous iso-porosity

region tool-path for the $(i+1)^{th}$ layer can be constructed by joining the set $Biarc(m)$ which may contain both linear and biarc segments. This technique is applied for all iso-porosity line segment as shown in Figure 7(a) and a contrast among smoothing is shown in Figure 7(b). The methodology is repeated for all the NL contours and stacking those contours consecutively one on top of the other will generate the 3D porous structure along with the optimum filament deposition path plan. By optimizing the porosity in each bi-layer set or pair, a true 3D spatial porosity can be achieved for the whole 3D structure.

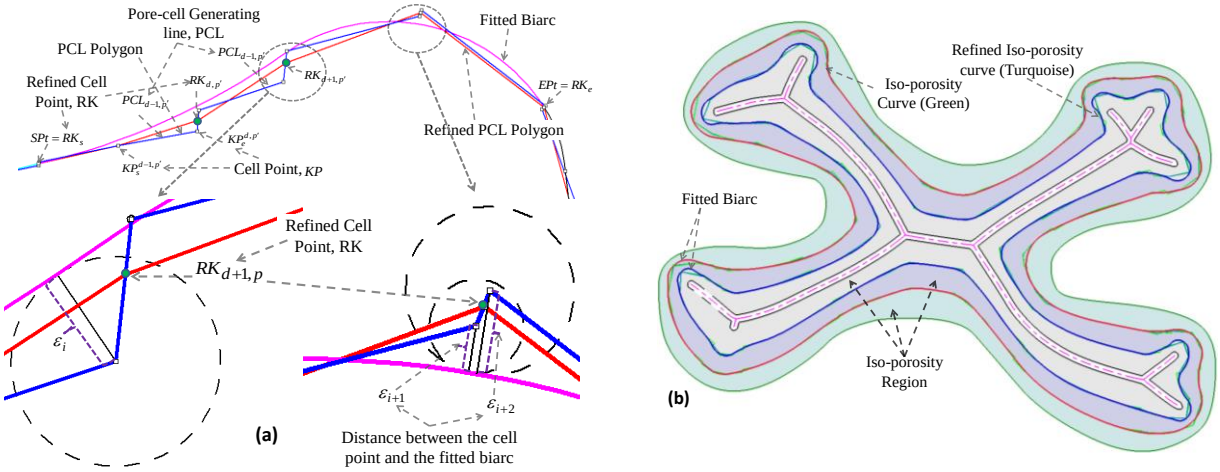

Figure 7 (a) Error control-based biarc fitting with refined points (b) Contrast between PCL polygon, refined PCL polygon and fitted biarc;.

4. Implementation

The proposed methodologies have been implemented with a 2.3 GHz PC using the Rhino Script and Visual Basic programming languages in the following examples. For a free-form shape geometry, the methodology generates a continuous tool-path for fabrication considering 8 iso-porosity regions (shown in Table 1) with constant; increasing and decreasing porosity are shown in Figure 8(a)-(c).

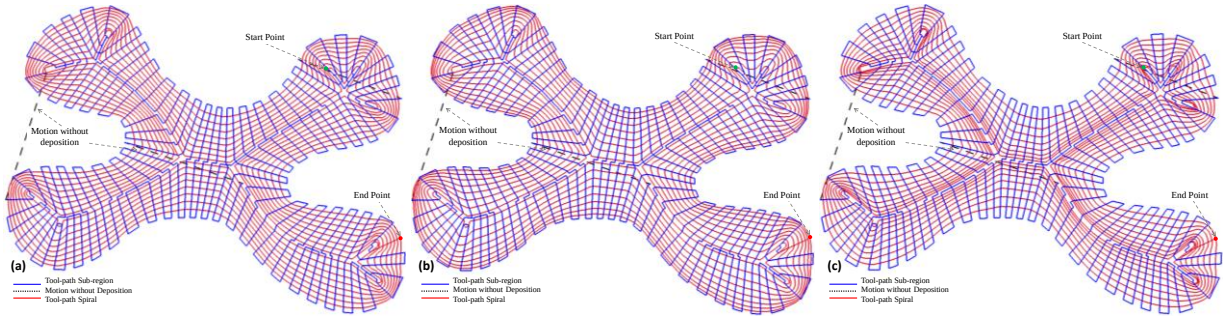

Figure 8 Tool-path generated with three pore cells in each sub-region (a) constant porosity (b) increasing, and (c) decreasing gradient porosity.

Table 1 Number of biarcs and porosity distribution for Figure 11(b)-(d).

Spiral Path Number(inner to outer)		1	2	3	4	5	6	7	8
Constant Porosity	Biarc No.	67	63	59	55	51	47	45	44
	Porosity	84	84	84	84	84	84	84	84
Increasing Gradient	Biarc No.	62	58	56	52	47	45	44	43
	Porosity	78	80	82	83	84	85	86	87
Decreasing Gradient	Biarc No.	72	68	62	55	50	46	45	44
	Porosity	87	86	85	84	83	81	80	79

The filament radius has been considered as 250 micrometer during the design processes. A total of 160 sub-regions have been generated from 3130 ruling lines, and a continuous tool-path has been constructed for bio-additive processes. Smoothing of iso-porosity line segments has been performed using biarcs and the total number of biarcs required is shown in Table 1. Finally, combining the tool-path for both the i^{th} and $(i+1)^{th}$ layers will make a continuous and interconnected tool-path for the designed bi-layer, as shown in Figure 8.

The methodology is also implemented on a femur head slice extracted using ITK-Snap 1.6 and Mimics Software. The following femur slice (shown in Figure 9) has been used to implement the methodology for variable but controllable porosity along its architecture. Figure 9(b) shows the generated medial axis and the corresponding medial boundary with $\delta = 0.5$ mm.

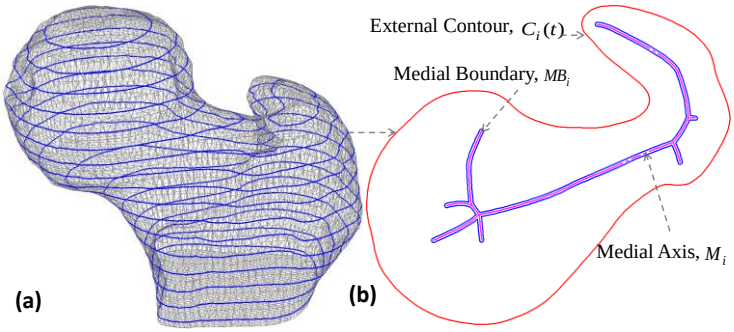

Figure 9 (a) Femur slice generation (b) medial axis and medial region construction.

A total of 105 sub-regions and three iso-porosity regions are generated with the methodology discussed above. Three sets of controllable porosity, i.e., constant, positive gradient and negative gradient porosity have been designed and fabricated with a 100 micrometer filament diameter as shown in Figure 10.

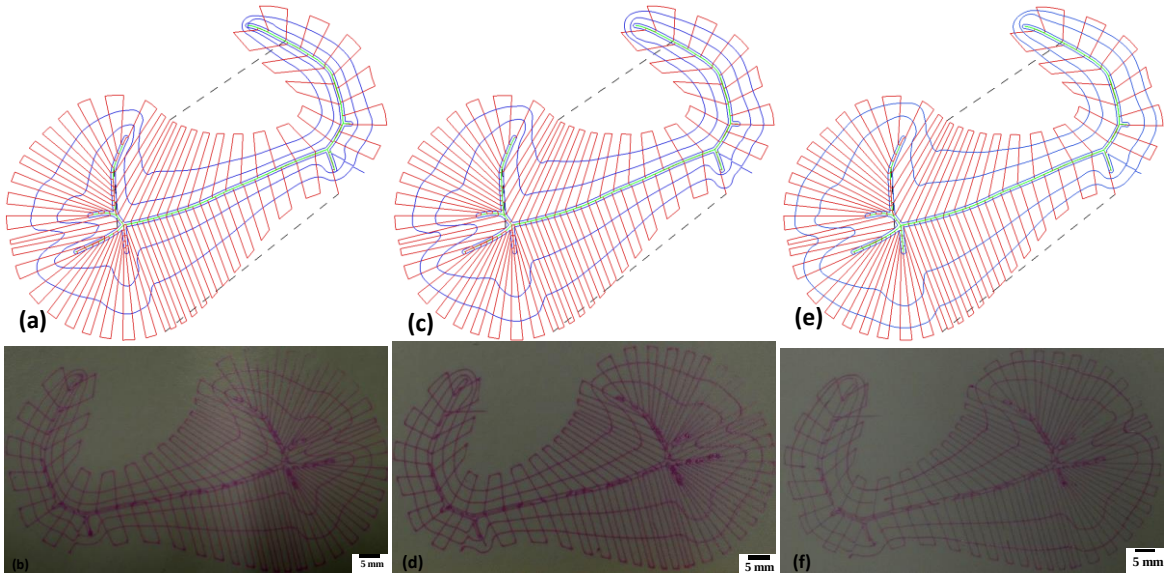

Figure 10 Model and fabrication for (a-b) decreasing gradient (c-d) constant porosity, and (e-f) increasing gradient.

As shown in Figure 10, a prototype computer numerical controlled (CNC) bio-additive fabrication system [15] is used because of the suitable fabrication parameters (pressure, temperature etc.) viable to deposit Sodium alginate, a type of hydrogel which is a bio-compatible materials. The fabricated structures closely conform to the design models. The proposed design algorithm generates the internal points of the designed scaffold sequentially. The developed methods can be used by any bio-additive processes.

5. Conclusion

The proposed methodology generates interconnected and controlled porous architecture with continuous deposition path planning appropriate for bio-additive fabrication processes. The proposed novel techniques can generate the scaffold structure with gradient (linear or non-linear), variational, or constant porosity that can provide localized control of material concentration along the scaffold architecture. Using layer-by-layer deposition method, a 3D porous scaffold structure with controllable variational pore size or porosity can be achieved by stacking the designed layers consecutively. Most importantly, the generated models are reproducible and suitable for any bio-additive fabrication processes.

References

[1] Jiang, C.-P., Huang, J.-R., and Hsieh, M.-F., 2011, "Fabrication of synthesized PCL-PEG-PCL tissue engineering scaffolds using an air pressure-aided deposition system," Rapid Prototyping Journal, 17(4), pp. 288 - 297.

[2] Yeo, M., Simon, C. G., and Kim, G., 2012, "Effects of offset values of solid freeform fabricated PCL-[small beta]-TCP scaffolds on mechanical properties and cellular activities in bone tissue regeneration," Journal of Materials Chemistry, 22(40), pp. 21636-21646.

[3] Freed, L. E., and Vunjak-Novakovic, G., 1998, "Culture of organized cell communities," Advanced Drug Delivery Reviews, 33(1–2), pp. 15-30.

[4] Taboas, J. M., Maddox, R. D., Krebsbach, P. H., and Hollister, S. J., 2003, "Indirect solid free form fabrication of local and global porous, biomimetic and composite 3D polymerceramic scaffolds," Biomaterials, 24(1), pp. 181-194.

[5] Khoda, A. B., and Koc, B., 2012, "Designing Controllable Porosity for Multifunctional Deformable Tissue Scaffolds," Journal of Medical Devices, 6(3), p. 031003.

[6] Sobral, J. M., Caridade, S. G., Sousa, R. A., Mano, J. F., and Reis, R. L., 2011, "Three-dimensional plotted scaffolds with controlled pore size gradients: Effect of scaffold geometry on mechanical performance and cell seeding efficiency," Acta Biomaterialia, 7(3), pp. 1009-1018.

[7] Khoda, A. K. M. B., Ozbolat, I. T., and Koc, B., 2011, "Engineered Tissue Scaffolds With Variational Porous Architecture," Journal of Biomechanical Engineering, 133(1), p. 011001.

[8] Lal, P., and Sun, W., 2004, "Computer modeling approach for microsphere-packed bone scaffold," Computer-Aided Design, 36(5), pp. 487-497.

[9] Schroeder, C., Regli, W. C., Shokoufandeh, A., and Sun, W., 2005, "Computer-aided design of porous artifacts," Computer-Aided Design, 37(3), pp. 339-353.

[10] Wettergreen, M. A., Bucklen, B. S., Starly, B., Yuksel, E., Sun, W., and Liebschner, M. A. K., 2005, "Creation of a unit block library of architectures for use in assembled scaffold engineering," Computer-Aided Design, 37(11), pp. 1141-1149.

[11] Kou, X. Y., and Tan, S. T., 2011, "Microstructural modelling of functionally graded materials using stochastic Voronoi diagram and B-Spline representations," International Journal of Computer Integrated Manufacturing, 25(2), pp. 177-188.

[12] Xu, S., Li, D., Lu, B., Tang, Y., Wang, C., and Wang, Z., 2007, "Fabrication of a calcium phosphate scaffold with a three dimensional channel network and its application to perfusion culture of stem cells," Rapid Prototyping Journal, 13(2), pp. 99–106.

[13] Li, X., Li, D., Lu, B., Tang, Y., Wang, L., and Wang, Z., 2005, "Design and fabrication of CAP scaffolds by indirect solid free form fabrication," Rapid Prototyping Journal, 11(5), pp. 312–318.

[14] Ku, S. H., Lee, S. H., and Park, C. B., 2012, "Synergic effects of nanofiber alignment and electroactivity on myoblast differentiation," Biomaterials, 33(26), pp. 6098-6104.

[15] Khoda, A. B., Ozbolat, I. T., and Koc, B., 2012, "Designing Heterogeneous Porous Tissue Scaffolds for Bio-Additive Processes (Under Review CAD-D-12-00309)." Journal of Computer Aided Design (CAD).

[16] Khoda, A., Ozbolat, I. T., and Koc, B., 2011, "A functionally gradient variational porosity architecture for hollowed scaffolds fabrication," Biofabrication, 3(3), pp. 1-15.

[17] Karande, T. S., Ong, J. L., and Agrawal, C. M., 2004, "Diffusion in Musculoskeletal Tissue Engineering Scaffolds: Design Issues Related to Porosity, Permeability, Architecture, and Nutrient Mixing," Annals of Biomedical Engineering, 32(12), pp. 1728-1743.

[18] Helmut, A., and Leonidas, J. G., 1996, "Discrete Geometric Shapes: Matching, Interpolation, and Approximation: A Survey," Institute of Computer Science, Freie Universitat, Berlin.